Smart Structures and Systems, *Vol. 28, No. 6 (2021) 745-760*
https://doi.org/10.12989/sss.2021.28.6.745

An algorithm for quantifying dynamic buckling and post-buckling behavior of delaminated FRP plates with a rectangular hole stiffened by smart (SMA) stitches

Ghazaleh Soltanieh*[1] and Michael C.H. Yam [2a]

[1] *Department of Building and Real Estate, Hong Kong Polytechnic University, Hong Kong, China*
[2] *The Chinese National Engineering Research Center (CNERC), 11 Yuk Choi Rd, Hung Hom, Hong Kong, China*

(*Received October 8, 2020, Revised July 5, 2021, Accepted September 16, 2021*)

Abstract. Dynamic buckling of structure is one of the failure modes that needs to be considered since it may result in catastrophic failure of the structure in a short period of time. For a thin fiber-reinforced polymer (FRP) plate under compression, buckling is an inherent hazard which will be intensified by the existence of defects like holes, cracks, and delamination. On the other hand, the growth of the delamination is another prime concern for thin FRP plates. In the current paper, reinforcing the plates against buckling is realized by using SMA wires in the form of stitches. A numerical framework is proposed to simulate the dynamic instability emphasizing the effect of the SMA stitches in suppressing delamination growth. The suggested algorithm is more accurate than the other methods when considering the transformation point of the SMA wires and the modeling of the cohesive zone using simple and yet reliable technique. The computational design of the method by producing the line by line orders leads to a simple algorithm for simulating the super-elastic behavior. The Lagoudas constitutive model of the SMA material is implemented in the form of user material subroutines (VUMAT). The normal bilinear spring model is used to reproduce the cohesive zone behavior. The nonlinear finite element formulation is programmed into FORTRAN using the Newmark-beta numerical time-integration approach. The obtained results are compared with the results obtained by the finite element method using ABAQUS/Explicit solver. The obtained results by the proposed algorithm and those by ABAQUS are in good agreement.

Keywords: Ari–Gur and Simonetta criterion; cohesive zone model; delamination; dynamic Buckling; FRP; shape memory alloy; stitches

1. Introduction

FRPs with a unique specification of adjustable properties is suitable to apply in different branches of engineering. The studies on stability of FRP plates under compressive loads (the buckling behavior) have been receiving attention (Kumar and Srinivasa 2020, Zare *et al*. 2020, Talebizadehsardari *et al*. 2020, Khorasani *et al*. 2020). In 1986, Leissa (1987) reviewed the early works on laminated composites under buckling loads. Kumar and Srinivasa (Kumar and Srinivasa 2020) conducted numerical and experimental studies on the global and local instability behavior of laminated plates.

Due to the manufacturing and/or architectural requirements, holes are often required for the connections of the plates. Nemeth *et al*. (1986) and Yasui and Tsukamura (1988) studied the buckling behavior of composite plates with a central circular or square cutout. They presented an approximate solution using trigonometric function for the displacement of the composite plates with the centrally located cutout. They showed that plates with circular holes have higher ultimate load carrying capability compared to plates with square holes (Baba 2007). The other research works on the buckling of an FRP plate with a hole (Aktas and Balcioglu 2013, Marshall 1987, Cafarova *et al*. 2017) have also paid attention to the important parameters such as ply orientations (Turvey and Sadeghipour 1987) and boundary conditions (Aktas and Balcioglu 2013). The stability related implications for the design of FRP plates under compressive load are divided in static and dynamic cases. The stability loss under the load in a very brief duration which is defined as dynamic buckling is more important in design than the former one (Xu *et al*. 1987). A timing diagram of the applied dynamic loads with a finite duration (pulse loading) may take a parabolic, sinusoidal (pressure from a wave of the sea), rectangular (mass hitting the structure, and then rebounded), and triangular (nuclear explosion) shapes (Kubiak 2013). The concept was first introduced in the early '30s with Euler buckling of columns (Koning and Taub 1934). In the '60s and early '70s, Budiansky (Budiansky 1962, Budiansky and Hutchinson 1966a, b) published the work on the dynamic buckling of the shells, while Volmir (Jankowski 2008) dealt with plate and shells. Budiansky introduced the criterion to determine the buckling load as a threshold at which the sudden unlimited deflection of the

*Corresponding author, Postdoctoral Fellow,
E-mail: gh-soltanieh@aut.ac.ir
[a] Professor, E-mail: michael.yam@polyu.edu.hk

ISSN: 1738-1584 (Print), 1738-1991 (Online)

structure in a very short period of time. FRP is one of the most vulnerable materials to delamination due to its weak mechanical properties in the transverse direction (Mahieddinet *et al*. 2015, Saboori *et al*. 2018, Torabi *et al*. 2020). The inter-laminar stiffness shows the approximate 2.5% of the stiffness in the fiber direction of composite (Nishimura and Aotani 1986). It is particularly important for the case of FRP plates with a hole. Holes are commonly used in FRP plates for connection which might cause the delamination and subsequently reducing the compressive strength of the plates. For plate under compressive load in the pre-buckling or buckling stages, the initiation of the delamination from the edge of the hole is one of the most serious problems (Nishimura and Aotani 1986). The structural stiffness loss due to delamination can reduce the load-carrying capacity of the plate while resulting in the subsequent propagation of the delamination and the final failure. Since mid-1980, interest has been attracted to the stitching technique for the through-the-thickness strengthening of FRP plates (Mouritz *et al*. 1997). Stitching is a unique method to provide high in-plane and transverse stiffness as well as improving the inter-laminar fracture toughness of structure for the prevention and suppression of delamination growth. It is proved that due to the improved fracture toughness (Dransfield *et al*. 1998, Jain and Mai 1995, Massabo and Cox 1999, Sankar and Sharma 1995) the stitched laminates show high resistance to delamination under impact (Dexter and Funk 1986, Caneva *et al*. 1993) as well as dynamic blast loads. In the review paper by Dransfield *et al*. (Dransfield *et al*. 1993) and Bibo and Hogg (1996), the improvement in impact and post-impact properties of the laminate were illustrated. They showed the effectiveness of stitching in reducing the growth of delamination around holes and cutouts on composite structures. The materials used for the stitches can be SMA wires, glass, carbon, and aramid threads. The efficiency of the SMA wires embedded in the FRP composite layers for instability (Bibo and Hogg 1996, Ibrahim *et al*. 2011, Soltanieh *et al*. 2017, 2019, Zhong *et al*. 1994), vibration control (Zhong *et al*. 2010, Ghaznavi and Shariyat 2017, Eyvazian *et al*. 2020) and damping under impact loads (Birman 2008, Lee *et al*. 2003, Zhang *et al*. 2021) has been reported in the literature. In 2004, Lau *et al*. (2004) investigated the efficacy of SMA stitch on FRP plates under low-velocity impact via experimental and numerical approaches. Recently, Cohades *et al*. (2018) have implemented the SMA stitches for self-recovery of the longitudinal cracks panel. They introduced this as a potential solution to control matrix cracking under impact loads. The study showed the reduction in damage in the form of the cracks and delamination because of the energy absorption of SMA wires. SMA stitch with its inherent energy absorbing behavior proved to be a good alternative in suppressing and healing the delamination (Manfredi *et al*. 2014). In this work, the dynamic buckling behaviors of SMA stitched FRP panels with a hole and the delamination are investigated. A computational framework for determining the instability limit loads and the post-instability paths of laminates with defects such as holes and delamination, is proposed using an exact algorithm (Soltanieh *et al*. 2018, Damanpack *et al*. 2015). One-dimensional Brinson model (Brinson 1993) is employed to simulate the super-elastic stress-strain relation of SMA wires. The complexity of the reciprocal relationship between the stress obtained from the buckling load and the SMA material specifications, and the three-dimensional behavior of SMA wires in the form of bilinear spring in the thickness direction of the plate were explained in a simple form using a flowchart. The procedure is coded in FORTRAN language. The adhesive properties are assumed as normal and shear springs in the energy formulation process using Hamilton's Principal. The Newmark-beta numerical time-integration approach is applied to solve the equations. The simplicity in implementation and time-saving of the proposed method is one of the advantages of the innovative method comparing to the use of commercial FE packages. The delamination propagation process is simulated using the cohesive zone model (CZM) (Elices *et al*. 2002) in ABAQUS. ABAQUS/Explicit solver is used for the transient dynamic analysis of the plate under impulse load. The good accordance between the results from the presented algorithm and those from the ABAQUS/Explicit shows the validity of the proposed method.

2. Formulation of the numerical framework

Dynamic buckling may occur when the structure is under load in a short period of time (the average value for the pulse duration equal to the period of natural vibration (Kowal-Michalska 2010). In the loading case of a very short period of time (less than the free vibration period) and very large magnitude, impact loading will happen, while for a long period (more than 1.5–2 times longer than the free vibration period) the load is called quasi-static. For solving the mathematical problem related to the dynamic buckling, Hamilton's principle is used to offer a methodical manner of deriving equations of motion of the plate (Baddour 2008).

$$\delta\Psi = \delta\int_{t_0}^{t_1} \Lambda\, dt = \delta\int_{t_0}^{t_1} (K - \Pi)\, dt = 0, \tag{1}$$

In the above equation K and Π are the kinetic and total potential energy of the system. The variation of kinetic energy is in the form of the below equation

$$\delta K = \rho\int_{\Omega} \delta U^T \ddot{U} d\Omega, \tag{2}$$

where U is the vector of displacements. In the integration domain (Ω), the area of the delamination and the hole are excluded.

The equation of the total potential energy can be written as the sum of the strain energy and the external work. The variation of the potential energy equation is shown in Eq. (3). In this equation, the first term refers to the variation of the strain energy. It is obtained from the multiplication of the transpose of the variation of the strain vector by the stress matrix. The second term demonstrates the external

work which is equal to the variation of the displacement vector multiplied by the external force vector (F_{ext}).

$$\delta\Pi = \int_{\Omega} \delta\epsilon^T \sigma d\Omega - \delta U^T F_{ext} \tag{3}$$

2.1 The governing equation of motion

Using the shear deformation plate theory, the matrix form of the von Karman strain-displacement relation (Shariyat *et al*. 2014) is expressed as

$$\epsilon = \begin{bmatrix} u_{0,x} + w_{0,x}^2 \\ v_{0,y} + w_{0,y}^2 \\ w_{0,y} + \phi_y \\ w_{0,x} + \phi_x \\ u_{0,y} + v_{0,x} + w_{0,x}w_{0,y} \end{bmatrix} + z\begin{bmatrix} \phi_{x,x} \\ \phi_{y,y} \\ 0 \\ 0 \\ \phi_{x,y} + \phi_{y,x} \end{bmatrix} = \Delta_1 U + z\Delta_3 U, \tag{4}$$

where the matrices Δ1 and Δ3 are defined in Eqs. (5) and (6), respectively (Shariyat *et al*. 2014).

$$\Delta_1 = \begin{bmatrix} \partial_{,x} & 0 & (w_{0,x})\partial_{,x} & 0 & 0 \\ 0 & \partial_{,y} & (w_{0,y})\partial_{,y} & 0 & 0 \\ \partial_{,y} & \partial_{,x} & (w_{0,x})\partial_{,y} + (w_{0,y})\partial_{,x} & 0 & 0 \end{bmatrix} \tag{5}$$

and

$$\Delta_3 = \begin{bmatrix} 0 & 0 & 0 & \partial_{,x} & 0 \\ 0 & 0 & 0 & 0 & \partial_{,y} \\ 0 & 0 & 0 & \partial_{,y} & \partial_{,x} \end{bmatrix} \tag{6}$$

The displacement matrix consists of five displacement elements.

$$U = \begin{bmatrix} u \\ v \\ w \\ \phi_x \\ \phi_y \end{bmatrix} \tag{7}$$

Substituting Eqs. (2) and (3) into Eq. (1), the differential equation of motion is written according to the displacement (U), its derivatives ($\dot{U}$), strain (ϵ), and stress (σ) matrices. Transforming the terms with $\dot{U}$ to $\ddot{U}$, and replacing the strain (ϵ) with the differential matrices (Eqs. (5) and (6)) multiplied by the displacement (U), and stress (σ) according to displacement, the equation of motion is written in form of the Eq. (8), (Shariyat *et al*. 2014). In Eq. (8), the variation of the total energy of the stitches ($\delta U^T K_{st}^m (\Delta_5)^T (\Delta_5)U$) is added and the shear ($\delta U^T K_S (\Delta_4)^T (\Delta_4)U$) and normal ($\delta U^T K_N (\Delta_5)^T (\Delta_5)U$) energy of the delaminated area (A_0) are subtracted (Phoenix *et al*. 2006).

$$\begin{aligned} &\int_{A_1} \delta U^T [I\ddot{U} + (\Delta_1)^T (A\Delta_2 + B\Delta_3)U \\ &+(\Delta_3)^T (B\Delta_2 + D\Delta_3)U + K^*(\Delta_4)^T (A^*\Delta_4)U \\ &+K_S(\Delta_4)^T (A^*\Delta_4)U + K_N(\Delta_5)^T (\Delta_5)U \\ &-F + K_{st}^m (\Delta_5)^T (\Delta_5)U] dA \\ &- \int_{A_0} [K_S(\Delta_4)^T (\Delta_4)U + K_N(\Delta_5)^T (\Delta_5)U] dA = 0 \end{aligned} \tag{8}$$

where A_1, K_{st}^m, K_S, and K_N are the domain of the integration equal to the area of the plate, stiffness of the stitches, shear and normal stiffness of the adhesive, respectively. A, B, D, and A* matrices are obtained from transformed stiffness matrix (Q_{ij}) (Soltanieh *et al*. 2018).

$$\begin{aligned} A_{ij} &= \int_{-h_2}^{h_2} \bar{Q}_{ij} dz, \\ B_{ij} &= \int_{-h_2}^{h_2} \bar{Q}_{ij} z dz, \\ A_{ij}^* &= \int_{-\frac{h}{2}}^{\frac{h}{2}} \bar{Q}_{ij} dz \qquad (i,j = 4,5) \end{aligned} \tag{9}$$

and the inertia matrix (I) as

$$I_i = \int_{\left(-\frac{h}{2}\right)}^{\left(\frac{h}{2}\right)} \rho(z)^{i-1} dz = \begin{bmatrix} I_1 & 0 & 0 & I_2 & 0 \\ 0 & I_1 & 0 & 0 & I_2 \\ 0 & 0 & I_1 & 0 & 0 \\ I_2 & 0 & 0 & I_3 & 0 \\ 0 & I_2 & 0 & 0 & I_2 \end{bmatrix} \quad (i = 1,2,3) \tag{10}$$

where K* is the shear correction factor equal to 5/6. Δ_2, Δ_4, and Δ_5 are defined as the differential matrices.

$$\begin{aligned} \Delta_2 &= \begin{bmatrix} \partial_{,x} & 0 & 0.5(w_{0,x})\partial_{,x} & 0 & 0 \\ 0 & \partial_{,y} & 0.5(w_{0,y})\partial_{,y} & 0 & 0 \\ \partial_{,y} & \partial_{,x} & (w_{0,x})\partial_{,y} + (w_{0,y})\partial_{,x} & 0 & 0 \end{bmatrix}, \\ \Delta_4 &= \begin{bmatrix} 0 & 0 & \frac{\partial}{\partial x} & 1 & 0 \\ 0 & 0 & \frac{\partial}{\partial y} & 0 & 1 \end{bmatrix}, \\ \Delta_5 &= \begin{bmatrix} 0 & 0 & 1 & 0 & 0 \\ 0 & 0 & -1 & 0 & 0 \end{bmatrix} \end{aligned} \tag{11}$$

The first term of Eq. (8) can be expressed as the mass matrix.

$$M = \int_{A_0} I dA \tag{12}$$

Introducing the structural stiffness of the laminate (K)

$$\begin{aligned} K = \int_A &[(\Delta_1)^T (A\Delta_2 + B\Delta_3) + (\Delta_3)^T (B\Delta_2 + D\Delta_3) \\ &+K^*(\Delta_4)^T (A^*\Delta_4) + K_S(\Delta_4)^T (A^*\Delta_4) \\ &+K_N(\Delta_5)^T (\Delta_5) + K_{st}^m (\Delta_5)^T (\Delta_5)] dA \end{aligned} \tag{13}$$

The external force vector is defined as

$$F_{ext} = F + \int_{A_0} [K_S(\Delta_4)^T (A^*\Delta_4)U + K_N(\Delta_5)^T (\Delta_5)U] dA \tag{14}$$

Eq. (8) takes the form of the equation of motion.

$$M\ddot{U} + C\dot{U} + KU = F_{ext} \tag{15}$$

2.2 Newmark-beta method

The Newmark-beta method is an implicit integration method to determine the displacement and velocity at every

time instance (Huebner *et al*. 2001).

$$U_{t+\Delta t}^{i+1} = U_t^i + \dot{U}_t^i \Delta t + \left[(0.5-\beta)\ddot{U}_t^i + \beta \ddot{U}_{t+\Delta t}^{i+1}\right]\Delta t^2$$
$$\dot{U}_{t+\Delta t}^{i+1} = \dot{U}_t^i + [(1-\alpha)\ddot{U}_t^i + \alpha \ddot{U}_{t+\Delta t}^{i+1}]\Delta t \quad (16)$$

The α and β parameters are assumed to be 1/2 and 1/4, respectively, for controlling the stability and accuracy of the method.

The incremental form of the equation of motion is

$$M\ddot{U}_{t+\Delta t}^{i+1} + R_{t+\Delta t}^{i+1} = F_{t+\Delta t} \quad (17)$$

The subscript t+Δt and superscript i+1 are used as the time and the iteration increment. The internal force vector ( ) can be expressed as

$$R_{t+\Delta t}^{i+1} = R_{t+\Delta t}^{i} + K\Delta U^{i+1} \quad (18)$$

The displacement vector and its first and second-time derivatives are computed from

$$U_{t+\Delta t}^{i+1} = U_{t+\Delta t}^{i} + \Delta U^{i+1}, \quad (19)$$

$$\dot{U}_{t+\Delta t}^{i+1} = a_1 \bar{U}^i - a_2 \dot{U}_t + a_3 \ddot{U}_t^i, \quad (20)$$

$$\ddot{U}_{t+\Delta t}^{i+1} = a_0 \bar{U}^i - a_1 \dot{U}_t - a_2 \ddot{U}_t \quad (21)$$

where

$$a_0 = \frac{1}{\beta \Delta t^2}, \quad a_1 = a_0 \Delta t,$$
$$a_2 = \frac{1}{2\beta} - 1, \quad a_3 = (1-\alpha)\Delta t \quad (22)$$

Convergence is reached when the following condition is satisfied

$$\frac{\Delta U^{i+1}(F_{t+\Delta t}^i - R_{t+\Delta t}^i - M\ddot{U}_{t+\Delta t}^i)}{\Delta U^1(F_{t+\Delta t} - R_{t+\Delta t}^0 - M\ddot{U}_{t+\Delta t}^0)} \le \varepsilon_E^r \quad (23)$$

ε_r^E is the preset energy tolerance.

2.3 Finite element formulation

To solve the problem by the finite element method, the elements of the equation of the motion are written for every element as

$$M^e = \int_{\Omega_0} N^T I N \quad (24)$$

$$K^e = \int_{A_0} [(N\Delta_1)^T (A\Delta_2 + B\Delta_3)N + (N\Delta_3)^T (B\Delta_2 + D\Delta_3)N + K^*(N\Delta_4)^T (A^*\Delta_4)N]dA \quad (25)$$

$$F^e = N^T {F_d}^e \quad (26)$$

In this study, the eight-node quadrilateral elements are implemented to avoid shear and membrane locking effects. The shape functions (N) are defined as

$$N_i = \frac{(1+\xi\xi_i)(1+\eta\eta_i)(\xi\xi_i + \eta\eta_i - 1)}{4} \quad (i = 1-4), \quad (27)$$

$$N_i = \frac{(1-\xi^2)(1+\eta\eta_i)}{4} \quad (i = 5,7), \quad (28)$$

$$N_i = \frac{(1+\xi\xi_i)(1-\eta^2)}{4} \quad (i = 6,8), \quad (29)$$

2.4 The constitutive equation of the super-elastic SMA

SMA stitches behavior is considered using the constitutive law of Brinson (1993). However, there are other 3D constitutive models which are very accurate in modeling the pseudo-elasticity of shape memory alloys regarding the martensite reorientation and thermo-mechanical coupling effects (Wang *et al*. 2017), but Because of modeling SMA in form of wires (one-dimension), the 1D Brinson model can precisely model the SMA behavior. The recurring stress-strain behavior of the super-elastic SMA makes a hysteresis loop. The forward part is related to phase change from austenite to martensite and backward from martensite to austenite, as shown in Fig. 1.

The loading section part has a bilinear path. After the start of phase transformation (σ_{MS}), the modulus of elasticity will decrease from σ_{MS} to σ_{MF}. For the dynamic loading in short period of time (impulse loading), the unloading stage in SMA is triggered by the sharp drop in reaction force of the plate. Again, the bilinear behavior at unloading stage causes the reduction in the modulus of elasticity after passing from σ_{AS} which will result in an increase of the in-plane deformation of the whole plate. Since the dynamic behavior is considered here, the damping effect of the SMA, which is obtained from the enclosed area by the hysteresis, will compensate the increase of the deformations at post-buckling. In general, Young's modulus is a function of the martensite fraction of the material. Regarding the transformation tensor, a relation between modulus is enforced by the residual strain (Brinson 1993). The stress from the martensite volume fraction of the stress

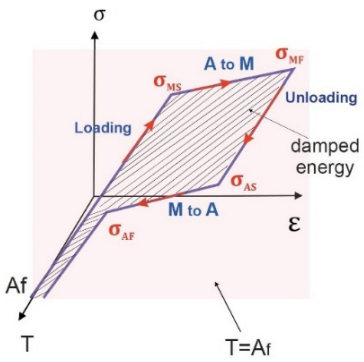

Fig. 1 The stress-strain-temperature curve of super-elastic shape memory alloy

(ξ_S) and the maximum recoverable strain (ϵ_L) has been reduced from the total stress.

$$\sigma = E(\varepsilon - \varepsilon_L \xi_S) \tag{30}$$

The modulus of elasticity of the SMA (E) consists of the EM and EA (the modulus of the SMA in the martensite and austenite phase).

$$E = E_A + \xi(E_M - E_A) \tag{31}$$

In the Brinson's model, the stress-strain relation in the transformation phase stage will be in the form of a cosine function, as it is shown in Eqs. (32) and (33). The stress-induced martensite fraction (ξ_S) for the super-elastic SMA (constant temperature) in the phase change from austenite to martensite is stated as:

(i) Forward phase change (A to M):

$$\xi_s = \frac{(1-\xi_{s_0})}{2} cos\left\{\frac{\pi}{\sigma_s^{cr} - \sigma_f^{cr}}\left(\sigma - \sigma_f^{cr} - C_M(T - M_s)\right)\right\} + \frac{(1+\xi_{s_0})}{2} \tag{32}$$

(ii) Backward phase change (M to A):

$$\xi_s = \frac{\xi_{s_0}}{2} cos\left\{\frac{\pi}{A_f - A_s}\left(T - A_s - \frac{\sigma}{C_A}\right) + 1\right\} \tag{33}$$

The combination of Voigt (iso-strain) and Reuss (iso-stress) micromechanical mixture rule is used for the mechanical properties of the hybrid composite materials (Rogers *et al*. 1991). In the below equations, V denotes the volume fraction; c and SMA indices are used for the composite and the SMA, respectively. The constants CM, and CA are the slopes of the critical stress-temperature curves for the austenite and the martensite phase transformations.

$$E_1 = E_{1C}V_C + E_{SMA}(1 - V_C) \tag{34}$$

$$E_2 = E_{2C}E_{SMA}/[E_{SMA}V_C + E_{1C}(1 - V_C)] \tag{35}$$

$$G_{12} = G_{12C}G_{SMA}/[G_{SMA}V_C + G_{12C}(1 - V_C)] \tag{36}$$

$$G_{13} = G_{13C}G_{SMA}/[G_{SMA}V_C + G_{13C}(1 - V_C)] \tag{37}$$

$$\nu_{12} = \nu_{12C}V_C + \nu_{12SMA}(1 - V_C) \tag{38}$$

$$\rho = \rho_C V_C + \rho_{SMA}(1 - V_C) \tag{39}$$

The strain vector is calculated from the equation below.

$$\varepsilon = \Delta_2 + z.\Delta_3.U \tag{40}$$

In the loading condition, at the positive stress zone, the strain and stress increase simultaneously (Eq. (41)). On the other hand, Eq. (42) shows the loading condition when the stress at SMA changes from negative to positive.

$$\left|\varepsilon^i\right| \geq \left|\varepsilon^{i-1}\right| \tag{41}$$

$$\varepsilon^i.\varepsilon^{i-1} < 0 \tag{42}$$

3. Solution algorithm

To trace the nonlinear unstable behavior, the iterative Newmark-beta method is employed to detect the exact instability point. The solution framework is shown in the flowchart, as shown in Fig. 2. The framework includes four blocks: i) Newmark-beta approach, ii) the phase detection of SMA, iii) the reciprocal relationship between the phase transformation and Newmark-beta method, and iv) the determination of the buckling load (BL). The phase detection block for the super-elastic SMAs has been first proposed by the first author and colleagues (Soltanieh *et al*. 2017, 2018).

According to the stress-strain diagram (Fig. 1), Young's modulus of the SMA is related to not only the stress magnitude but the loading or unloading states. In the flowchart, the phase states are described for the loading/unloading conditions. Three limits of the strains at the start or finish phase transformations are defined for the loading case.

$$\left|\varepsilon^i\right| \leq \varepsilon^{Ms} \tag{43}$$

$$\varepsilon^{Ms} < \left|\varepsilon^i\right| \leq \varepsilon^{Mf} \tag{44}$$

$$\left|\varepsilon^i\right| \geq \varepsilon^{Mf} \tag{45}$$

For unloading, four limit are defined as

$$\left|\varepsilon^i\right| \geq \varepsilon^{As} \tag{46}$$

$$\varepsilon^{Af} < \left|\varepsilon^i\right| \leq \varepsilon^{As} \tag{47}$$

$$\left|\varepsilon^i\right| \leq \varepsilon^{Af} \tag{48}$$

$$\left|\varepsilon^i\right| \leq \varepsilon^{Ms} \tag{49}$$

The smooth flag-shaped stress-strain hysteresis during the vibration of the plate under dynamic loads cannot explain the changes in stress inside the loop. These oscillations do not include any phase transformations. The misdetection of the SMA phases in each step will dramatically affect the final result since there is a coupled relationship between the SMA modulus and the obtained displacements from the Newmark-beta method. Regarding the declaration of the exact phase, indicators are set to show the entering ($Indic^i$) and exiting ($IndicE^i$) of the loop or demonstrating the oscillation at the loading ($IndicSL^i$) or unloading ($IndicSU^i$). These are the important keys to understand the exact behavior of the SMA in cases of the phase transformation (for more details, refer to Fig. 2).

In the fourth block (purple box, Fig. 2), the obtained maximum displacements (W_m) of the panel versus the corresponding applied load (F) curve would be constructed (Fig. 3). The Ari–Gur and Simonetta criteria (Ari-Gur and Simonetta 1997) is well suited for use in the dynamic pulse buckling of the rectangular composite plate. According to

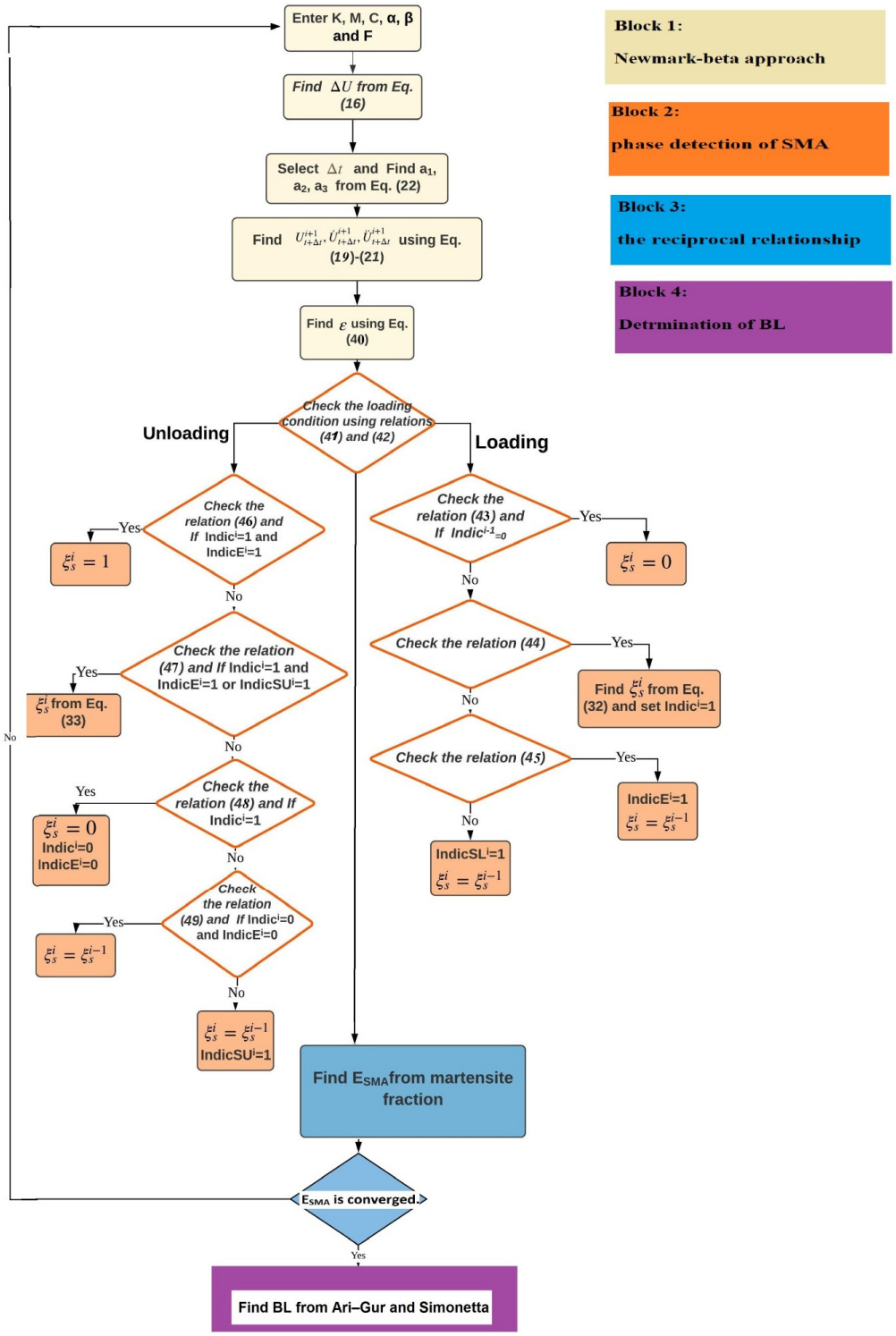

Fig. 2 The framework for solving Eq. (15)

Ari–Gur and Simonetta criteria, dynamic buckling occurs when a small increase in the amplitude of the pulse load causes a great increase in the value of the deflection.

4. Result and discussion

In this section, the presented algorithm is validated against the results from the literature. After verifying the method, the negative impact of the presence of a hole as well as the positive influence of the SMA stitches with the super-elastic behavior on buckling capacity, post-buckling behavior, and delamination growth are investigated. A parametric study is carried out to examine the influence of the host FRP lay-ups and the volume fraction of the SMA on the effectiveness of the super-elastic SMA stitches.

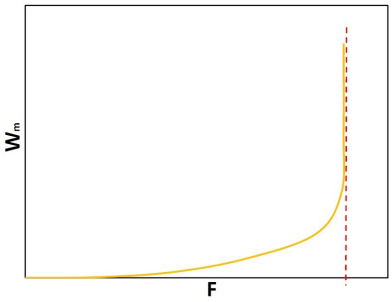

Fig. 3 Maximum displacement versus critical load (Ari–Gur and Simonetta criteria)

4.1 Newmark-beta method

To verify the present approach and the algorithm, the results of a plate with the pre-supposed delamination at two specific positions without any stitches (Fig. 4) are compared with the experimental (Alfano and Crisfield 2001) and numerical results (ABAQUS 2014). The model includes an FRP plate with a cantilever boundary condition with delamination under the transversely applied displacement directed upward for the upper part of the beam and downward for its lower part at the free edge, as shown in Fig. 4. The FRP is considered to have a uni-directional orientation with 24 layers in 0 degrees (024). This example is a prototype for fracture characterization (double cantilever beam (DCB) under the transverse displacement) (Sekiguchi *et al*. 2017). The mechanical properties of the FRP and adhesive are shown in Table 1. For simplification in simulation, the mechanical properties of matrix and fibers are not considered separately. For investigation of the growth of pre-supposed delamination, the strengths of the FRP in normal, and two shear modes are explained in terms of N0, T0, and S0 and no details for the breakage strength of matrix and fibers separately (Alfano and Crisfield 2001). Using LEFM, the visco-elastic properties of polymer and fibers are neglected (Zhao 2011).

The geometrical specifications are depicted in Fig. 4.

The type of elements for the FRP and adhesive (Fig. 5) are C3D8R (8-node linear brick, reduced integration) and COH3D8 (8-node three-dimensional cohesive element), respectively.

The cohesive zone model (CZM) is implemented based on the traction-separation law (see Fig. 6). The bilinear traction-separation constitutive law (Geubelle and Baylor 1998) is applied.

The quadratic failure criterion (QUADS damage) is selected for the delamination growth in the cohesive

Table 1 The properties of FRP composite (Alfano 2001) and adhesive layer (Elices 2002)

	E_1 (GPa)	E_2 (GPa)	E_3 (GPa)	ν_{12}	ν_{13}	ν_{23}	G_{12} (GPa)	G_{13} (GPa)	G_{23} (GPa)	ρ (Kg/m^3)
FRP	115	8.5	8.5	0.29	0.29	0.3	4.5	3.3	4.5	2.0388×10^6
	E (MPa)	G_1 (MPa)	G_2 (MPa)	N_0 (MPa)	T_0 (MPa)	S_0 (MPa)	G_{Ic} (N/m)	G_{IIc} (N/m)	G_{IIIc} (N/m)	ρ (Kg/m^3)
Adhesive	850	850	850	3.3	7	7	0.33×10^3	0.8×10^3	0.8×10^3	1.5291×10^6

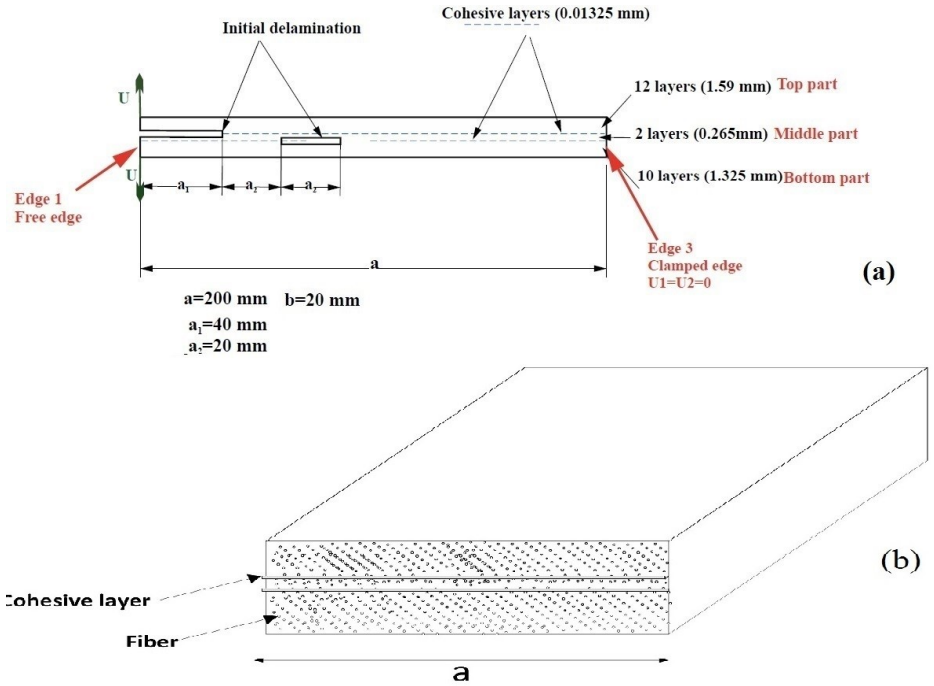

Fig. 4 Geometry of the verification example

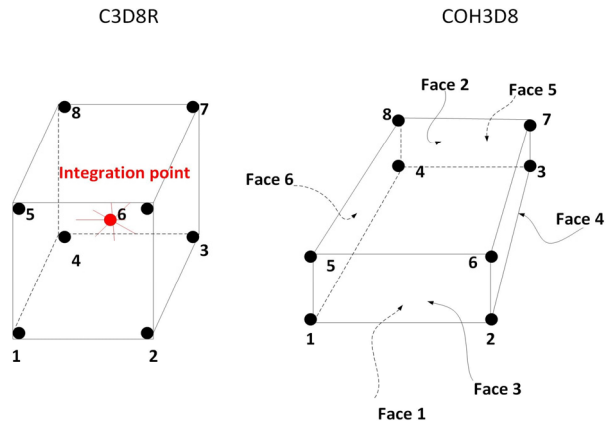

Fig. 5 C3D8R (8-node linear brick, reduced integration) and COH3D8 (8-node three-dimensional cohesive element)

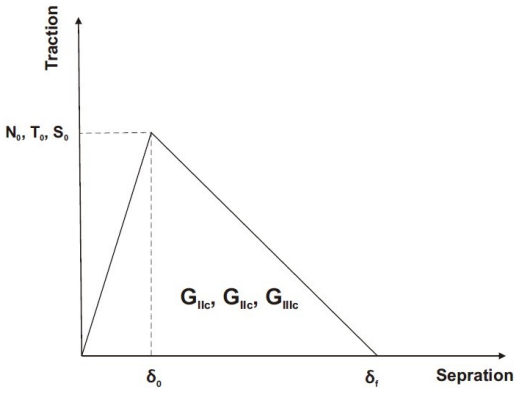

Fig. 6 Bilinear traction-separation law

elements (Ye 1988).

$$\left(\frac{\langle N\rangle}{N_0}\right)^2+\left(\frac{T}{T_0}\right)^2+\left(\frac{S}{S_0}\right)^2=1 \tag{50}$$

N, T, and S are normal (perpendicular to the interface) and two shear interfacial tractions (tangential to the interface), while N_0, T_0, and S_0 are their corresponding strengths. The angle bracket is used to show that only positive normal tractions contribute to the failure criterion. The reaction force versus the out-of-plane displacement of the free edge (maximum deflection) is depicted in Fig. 7. It shows a satisfactory comparison between the obtained results of the present algorithm, the ABAQUS benchmark example (ABAQUS 2014) and the experimental results (Alfano and Crisfield 2001) before 20 mm of displacement. The experimental results and the present algorithm follow a similar pattern. However, after 20 mm, a sharp drop of loads was observed in both numerical results which was related to the sudden failure of a relatively large number of cohesive elements in a very short period of time (ABAQUS 2014). However, the drop in the experimental load was comparatively small.

4.2 Dynamic buckling of delaminated plate without hole

Based on the above validated FE modelling technique, a FE model to examine the dynamic buckling of an FRP plate was developed. The compressive in-plane displacement is applied to the free edge of the previous example (refer to Fig. 4) for analyzing the dynamic buckling. The results will be used as a benchmark to be compared with the results of the plate with a hole. Three types of dynamic impulse are assumed, namely, rectangular, half-sinusoidal, and triangular, as shown in Fig. 8. The dynamic buckling occurs for the impulse duration near the natural period of longitudinal vibration of structure and with a mode corresponding to the static buckling mode.

The results are presented for two cases, namely, with stitches and without stitches. Two longitudinal SMA stitches are placed in 7.5 mm distance from the horizontal edges for the case with stitches. The volume fraction of SMA to the total volume is considered to be 5%. The diameters of the stitches are assumed to be 0.2, 0.4, and 0.6 mm for 0.5, 1, and 1.5%. The mechanical properties of the SMA is given in Table. 2.

For simulating the SMA stitches in ABAQUS, the SLIPRING connectors are used in the thickness direction

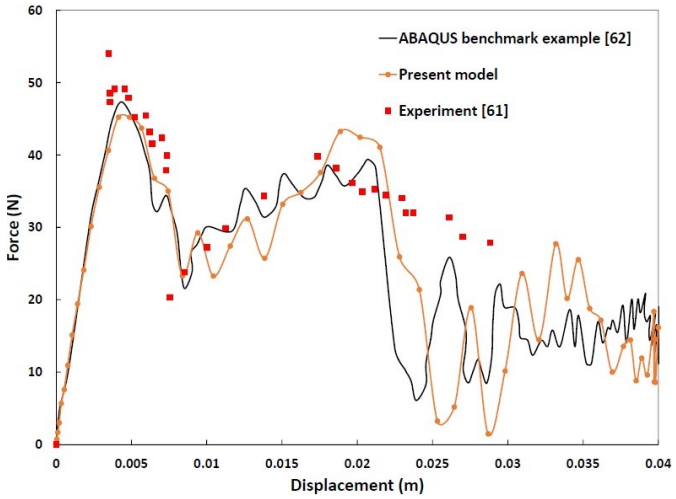

Fig. 7 Validity of the presented algorithm against the literature (ABAQUS 2014)

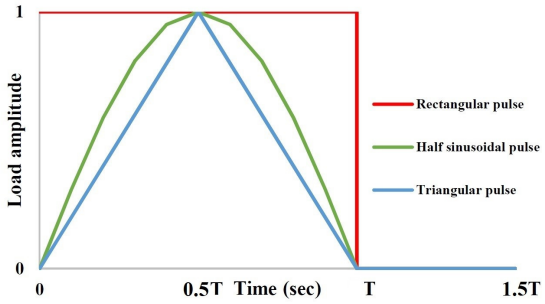

Fig. 8 Time history of the applied loads

for the SMA which pass through the delaminated area (Riccio *et al*. 2017). The SMA wires in the other sections are simulated with the AXIAL connectors (see Fig. 8).

According to Ari–Gur and Simonetta criterion, the diagrams of the maximum out-of-plane deflection versus in-plane reaction force for different shapes of the time history (Triangular, half-sinusoidal and rectangular) of the plate with (0.5% of volume fraction) and without stitches are shown in Fig. 10. Buckling occurs when, for a given pulse shape and duration, a small increase in the pulse intensity causes a sharp increase in the edge lateral deflection (Ari-Gur and Simonetta 1997). The maximum BLs among the three different time-histories (Fig. 8) are obtained for triangular shape of time-history. The reason behind of being maximum is the minimum area beneath the time history (Petry and Fahlbusch 2000). With the same analogy the minimum buckling load related to rectangular time-history shape.

The increase in BLs for the stitched plate compared to the unstitched plate are 55%, 49% and 50 % for the rectangular, half-sinusoidal and triangular shape time-histories, respectively.

4.3 Dynamic buckling of delaminated plate with a hole

Two cases of stitched and unstitched plate with a hole are considered here. The geometric configuration of the

Table 2 The properties of Nickel Titanium alloy (Brinson 1993)

	E_A (GPa)	E_M (GPa)	ν	α_A (K^{-1})	α_M (K^{-1})	M^S (K)	M^A (K)	A^S (K)	A^f (K)	ε_L	T_0 (K)	ρ (Kg/m^3)
SMA	70	30	0.33	22×10^{-6}	22×10^{-6}	291	271	295	315	0.05	253	6.45×10^6

(a) (b)

Fig. 9 Connection type (a) SLIPRING; (b) AXIAL (Riccio 2017)

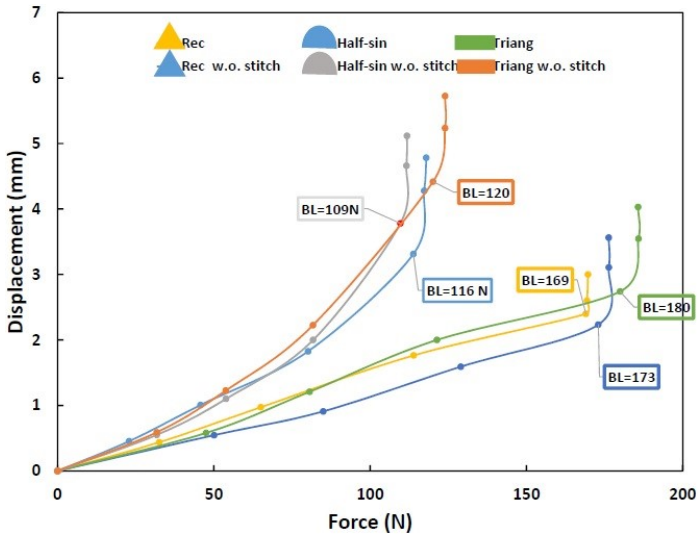

Fig. 10 The in-plane reaction force versus maximum out-of-plane displacement of the plate without hole, with and without SMA stitch

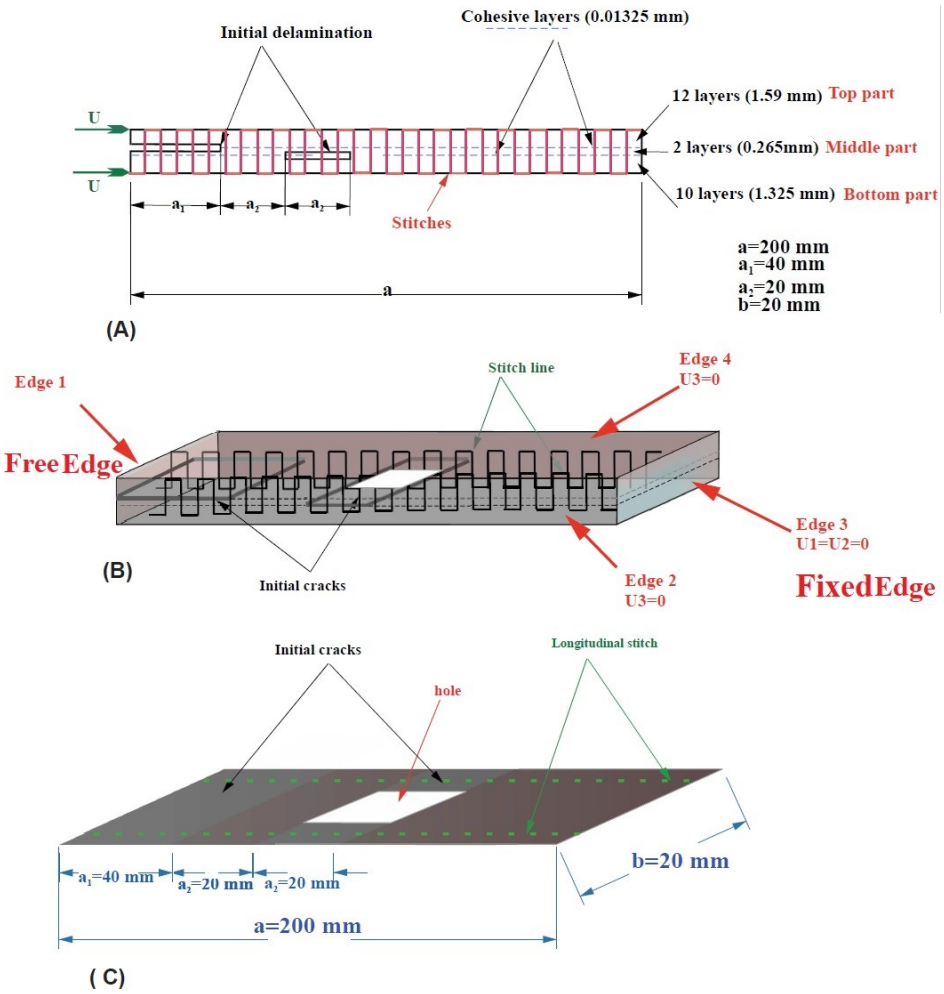

Fig. 11 Longitudinally stitched composite with two delamination and a square hole: Middle section through the stitches, (B) 3-D view, and (C) Top view (Alfano and Crisfield 2001)

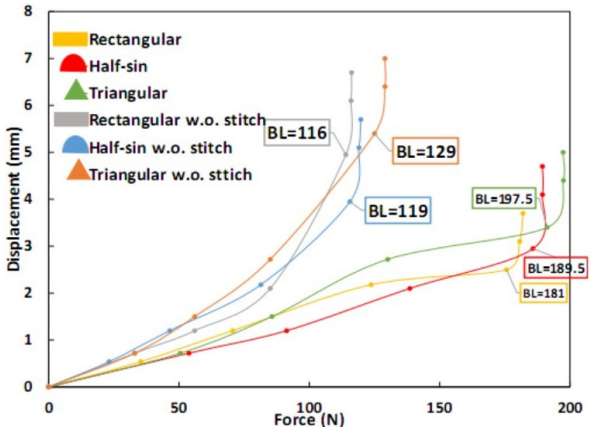

Fig. 12 The in-plane reaction force versus maximum out-of-plane displacement of the plate with a hole, with and without SMA stitch

plate is shown in Fig. 11. The square hole with the size of 5 millimeters is located at 70 mm from the free edge and in the middle of the delamination. It has the depth equal to the thickness of the plate. The plate has the cantilever boundary conditions. Two lines of the SMA stitch are placed in the middle of the free horizontal edge and the edge of the hole longitudinally.

The in-plane reaction forces versus maximum out-of-plane displacements of the plate are depicted in Fig. 11. As shown in the figure, the maximum dynamic buckling loads (sharp increase in deflection) are observed for the triangular pulse cases.

The results for the buckling load of the plates with and without stitches are shown in Table. 3. The increase in BLs are observed as 56%, 59% and 53% for the rectangular, half-sinusoidal and triangular shape time-histories, respectively.

Table 3 The buckling loads of laminates with different impulse shapes

Rectangular pulse		Rectangular pulse		Rectangular pulse	
BL w.o. stitch (N)	BL w stitch (N)	BL w.o. stitch (N)	BL w stitch (N)	BL w.o. stitch (N)	BL w stitch (N)
116.06	180.7	119.21	189.45	129.33	197.5

Table 4 The buckling loads of laminates with different lay ups

	Rectangular pulse		Half-sin pulse		Triangular pulse	
Stacking sequence	BL w.o. stitch (N)	BL w stitch (N)	BL w.o. stitch (N)	BL w stitch (N)	BL w.o. stitch (N)	BL w stitch (N)
$(0)_{12}$	116.06	180.7	119.21	189.45	129.33	197.5
$(-45)_{10}/0_2/(+45)_{12}$	47.12	65.5	49.08	69.22	55.43	76.49
$(90)_{10}/0_2/(90)_{12}$	39.41	55.1	41.83	58.14	45.88	63.33

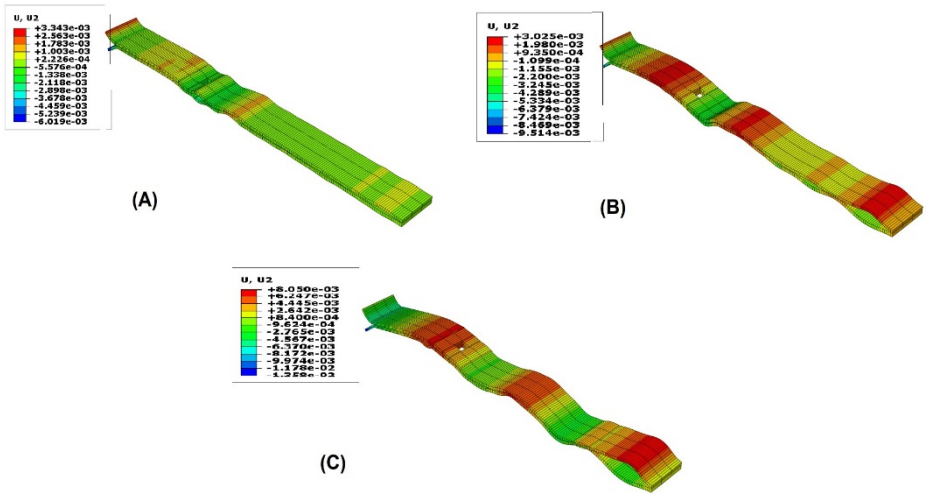

Fig. 13 Out-of-plane deformation of the plate at the different instances: (A) Buckling instance; (B) Post-buckling stage; (C) End of simulation

4.4 Dynamic buckling of stitched delaminated plate with a hole for different layups of the host FRP plate

To show the effect of the other factors on the efficacy level of the SMA stitches, a parametric study is carried out to examine the effects of the different layups of the host composite plates. The stitch is placed longitudinally in the laminate. The buckling load and the deflection of the plates with different layups are shown in Table 4. Depending on the stacking sequence of the composite, the SMA could increase the buckling load for the cases up to 60 percent. The maximum increase is related to the unidirectional (0_{24}) layup, under the rectangular impulse load.

The deformed plate with stitches under rectangular impulse load at the buckling and post-buckling instances are shown in Fig. 12. The results illustrate the good influence of the SMA stitches on the delamination growth suppression after buckling occurrence at the end of simulation.

4.5 Dynamic buckling of stitched delaminated plate with a hole with different volume fractions of the SMA

The beneficial effect of the 5% volume fraction of SMA stitches on the buckling capacity of the plates has been elaborated in the previous section. Since the SMA material used has a smaller young modulus both in the austenite and the martensite phases than that of the FRP, using the SMA stitches more than a certain volume fraction might have negative effect on the buckling capacity of the plates. To further examine the effect of SMA volume fraction, the plate is stitched with three different volume fractions of SMA wires (0.5, 1, and 1.5%). The diameters of the wires are changed to have different volume fractions while the numbers and the position of wires are kept the same. The plate with 0.5 % of SMA increase the buckling capacity up to 60%. However, the data from Table 5 shows that more SMA does not always result in a better effect. Due to the

Table 5 The buckling loads of laminates with different volume fraction of SMA

	Rectangular pulse		Half-sin pulse		Triangular pulse	
Volume fraction	BL w.o. stitch	BL w stitch	BL w.o. stitch	BL w stitch	BL w.o. stitch	BL w stitch
	(N)	(N)	(N)	(N)	(N)	(N)
0.5%	116.06	180.7	119.21	189.45	129.33	197.5
1%	116.06	185	119.21	191.25	129.33	199.01
1.5%	116.06	179.9	119.21	190	129.33	196.89

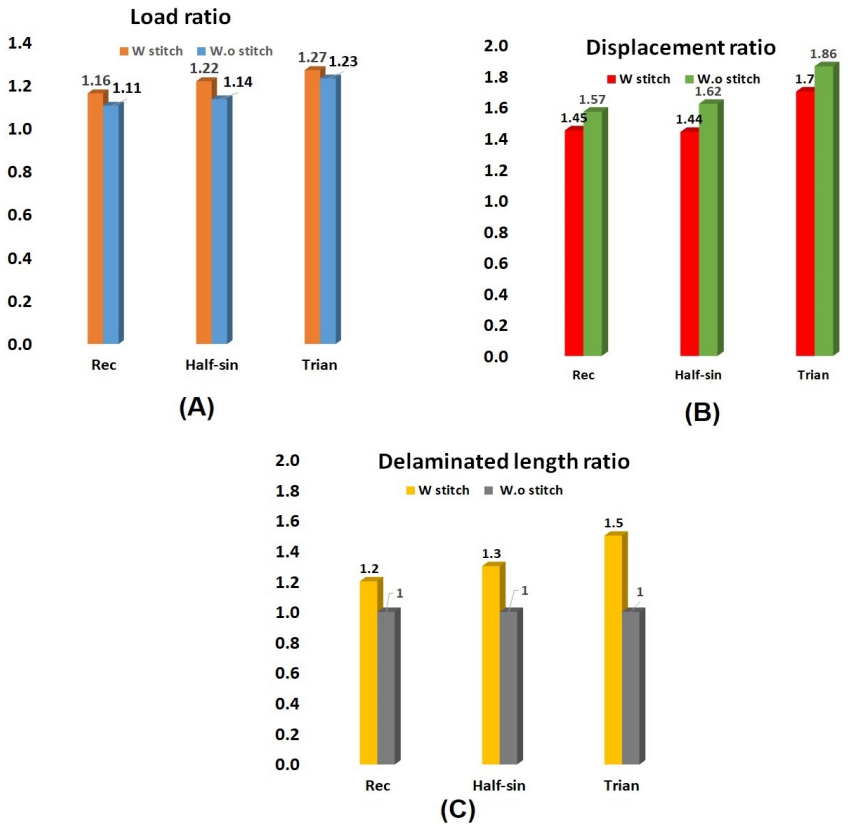

Fig. 14 The ratios: (A) Load; (B) Displacement; and (C) Delaminated length for the plate without hole

low normal modulus (E1) of the SMA, for the plates with 1% SMA respect to the plates with 0.5% SMA the BLs will be increased up to 2%. For the plate with 1.5% of SMA the BLs are obtained less than the results for 1%. This means that the damped energy from the super-elasticity cannot compensate the negative influence of the SMA on the reduction of the stiffness of the stitched plate for the amount of the SMA fractions.

4.6 Discussion of results

The results for BL, the deformation at the buckling instant and the delamination growth are summarized and discussed here. The effect of the stitch on the plate without hole is considered. The load ratio (dynamic critical load to static load), as well as the deformation ratio (maximum lateral displacement at the dynamic buckling to the related value at the static buckling instant) obtained from the proposed algorithm for the case of unidirectional (024) laminates under the different impulse loads are depicted in Fig. 14 part (A) and (B). The static buckling loads for the plate with and without stitches are equal to 155.4 and 105 (N). The dynamic buckling load for each case is obtained from the ratios shown in the graphs of Fig. 14(A). The displacements for the plate with and without stitches are equal to 2.2 and 2.9 (mm). The corresponding ratios can be obtained from Fig. 14(B). The ratios for the relevant lengths of the delaminated area at the end of the simulation are also shown in part (C).

According to the buckling load ratios for the plates which are higher than one (between 1.2-1.4 times of the static loads), the dynamic buckling (impulse loading in the period of equal to the natural period) occurs with higher value than the static buckling (loading in the duration larger than natural period). The buckling loads, displacements and delaminated lengths at the dynamic buckling instants are larger compared with those of the static buckling instants. For the case of the plate without stitch, the delamination grew till final rupture of the structure in both dynamic and static cases, then the ratio remains equal to one. The results illustrate the highest buckling load for triangular time-history for both cases of without and with stitches. The beneficial effects of stitching on increasing the BL, decreasing the deformation and delamination growth are obvious when comparing the results for the cases of without and with stitches.

The ratios of the plate with a hole are depicted in Fig. 15. Comparing Figs. 15 and 14 illustrates that the stitches in the plate with a hole contribute more in increasing buckling load capacity of the plate in dynamic impulse loads than the plate without hole. However, the deformation and the delaminated length ratios are larger for the plate with a hole. This illustrates the negative effect of the SMA in increasing deformation and delamination accompanied with the positive effect of it in increasing the buckling load for the plate with a hole.

ItshouldbenotedthatinthisresearchtheBLsareobtainedfro mthepresentedalgorithm. ABAQUS is used here for illustrating the deformed shape of the plate. Conducting the FE analysis with ABAQUS will require up to 162 hours, while one-third of this time (50 hours) will be needed for the proposed algorithm.

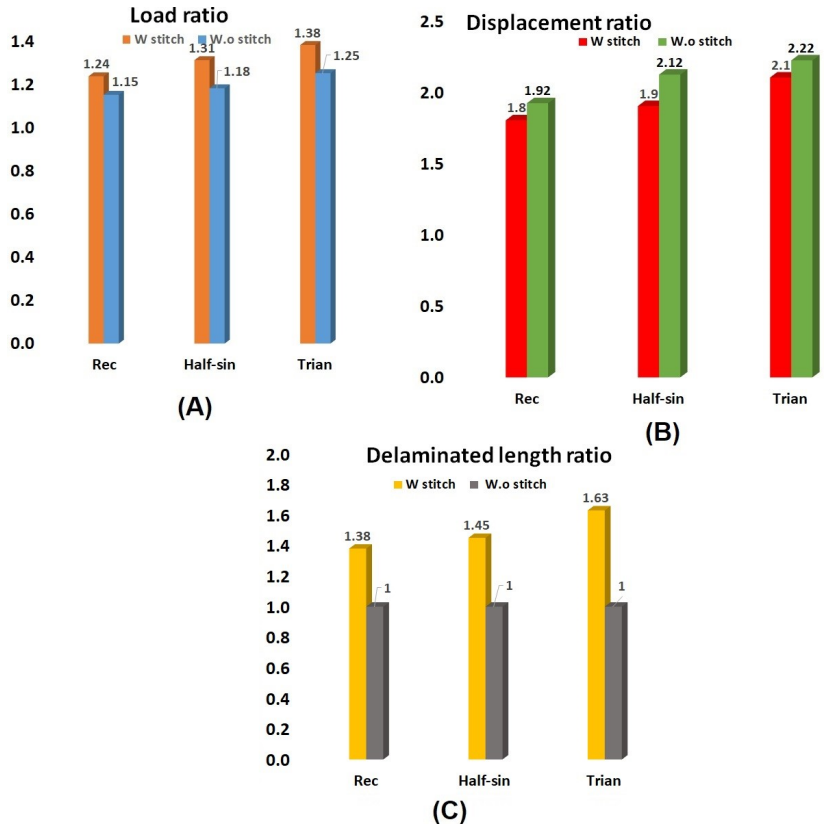

Fig. 15 The ratios: (A) Load; (B) Displacement; and (C) Delaminated length for the plate with a hole

5. Conclusions

The SMA stitches are used in this research for increasing the dynamic buckling capacity and the delamination growth suppression of delaminated FRP plate with a hole. To analyze dynamic buckling problem considering the delamination growth, the conventional approach using FE analysis is computational demanding. To deal with this issue, an algorithm is proposed to evaluate the dynamic buckling behavior of FRP plates with a hole and SMA stitches. The proposed method was simply programmed in FORTRAN. It is easily comprehensible for the complicated phase transformation behavior of the SMA material. Following conclusions can be drawn from the case studies:

(i) Using the algorithm takes less time than conducting the FE analysis with ABAQUS (almost 1/3 of the time).
(ii) The good impact of stitching on strength of the plate against dynamic instability is observed with the maximum 60 percent increase of the Buckling loads.
(iii) The time-history shapes of the impulse load will influence the efficacy of the SMA in increasing the BL values. For the rectangular shape impulse (the most area beneath the load-time graph), the BLs and the related deflections are the minimum comparing to those of the triangular and half-sinusoidal.
(iv) The stacking sequence of the host FRP laminates affects the increase of the buckling load due to stitches. The rate of increase of BL obtained is 55 percent for the unidirectional, while 39 percent for the $(-45_{10}/0_2/+45_{12})$ is observed.
(v) The efficiency of SMA stitches in increasing the BLs is more in the plate with a hole than the plate without a hole.
(vi) The plates show more resistant to dynamic buckling than the static buckling (the ratio of dynamic BL to static BL is obtained up to 1.38).
(vii) The deformation and delaminated length of the dynamic buckling case were larger than those of the static buckling case (the maximum ratios for deformation and delaminated length are 2.22 and 1.63, respectively.)

Acknowledgments

This research is funded by a grant from the Chinese National Engineering Research Centre for Steel Connection, The Hong Kong Polytechnic University (Project No. 1- BBV 4).

References

Abaqus, V.6.14 (2014), 6.14 Documentation, Dassault Systemes Simulia Corporation.
Aktas, M. and Balcioglu, H.E. (2013), "Buckling behavior of pultruded composite beams with circular cutouts", *Steel*

Compos. Struct., *Int. J.*, **17**(4), 359-370. https://doi.org/10.12989/scs.2014.17.4.359

Alfano, G. and Crisfield, M.A. (2001), "Finite element interface models for the delamination analysis of laminated composites: mechanical and computational issues", *Int. J. Numer. Meth. Eng.*, **50**, 1701-1736. https://doi.org/10.1002/nme.93

Ari-Gur, J. and Simonetta, S.R. (1997), "Dynamic pulse buckling of rectangular composite plates", *Compos. Part B Eng.*, **28**, 301-308. https://doi.org/10.1016/S1359-8368(96)00028-5

Baba, B.O. (2007), "Buckling behavior of laminated composite plates", *J. Reinf. Plast. Compos.*, **26**, 16371655. https://doi.org/10.1177/0731684407079515

Baddour, N. (2008), "Hamilton's principle for the derivation of equations of motion, Leading-Edge", *Appl. Math. Model. Res.*, 155-182.

Bibo, G.A. and Hogg, P.J. (1996), "The role of reinforcement architecture on impact damage mechanisms and post-impact compression behaviour", *J. Mater. Sci.*, 3b1, 1115-1137. https://doi.org/10.1007/BF00353091

Birman, V. (2008), "Shape memory elastic foundation and supports for passive vibration control of composite plates", *Int. J. Solids Struct.*, **45**, 320-335. https://doi.org/10.1016/j.ijsolstr.2007.08.023

Brinson, L.C. (1993), "One-dimensional constitutive behavior of shape memory alloys: thermo mechanical derivation with non-constant material functions and redefined martensite internal variable", *J. Intell. Mater. Syst. Struct.*, **4**(2), 229-242. https://doi.org/10.1177/1045389X9300400213

Budiansky, B. (1962), "Axisymmetric dynamic buckling of clamped shallow spherical shells", *NASA TN*, **1510**, 597-606.

Budiansky, B. and Hutchinson, J.W. (1966a), "Dynamic buckling of imperfection-sensitive structures", In: *Applied Mechanics*, pp. 636-651.

Budiansky, B. and Hutchinson, J.W. (1966b), "Dynamic buckling estimates", *AIAAJ*, **4**(3), 525-530. https://doi.org/10.2514/3.3468

Cafarova, F.I., Akbarov, S.D. and Yahnioglu, N. (2017), "Buckling delamination of the PZT/Metal/PZT sandwich circular plate disc with penny-shaped interface cracks", *Smart Struct. Syst.*, *Int. J.*, **19**(2), 163-179. https://doi.org/10.12989/sss.2017.19.2.163

Caneva, C., Olivieri, S., Santulli, C. and Bonifazi, G. (1993), "Impact damage evaluation on advanced stitched composites by means of acoustic emission and image analysis", *Compos. Struct.*, **25**, 121-128. https://doi.org/10.1016/0263-8223(93)90158-M

Cohades, A., Hostettler, N., Pauchard, M., Plummer, C.J.G. and Michaud, V. (2018), "Stitched shape memory alloy wires enhance damage recovery in self healing fibre-reinforced polymer composites", *Compos. Sci. Technol.*, **161**, 22-31. https://doi.org/10.1016/j.compscitech.2018.03.040

Damanpack, A.R., Bodaghi, M., Liao, W.H., Aghdam, M.M. and Shakeri, M. (2015), "A simple and efficient 1- D macroscopic model for shape memory alloys considering ferro-elasticity effect", *Smart Struct. Syst.*, *Int. J.*, **16**(4), 641-665. https://doi.org/10.12989/sss.2015.16.4.641

Dexter, H. and Funk, J. (1986), "Impact resistance and interlaminar fracture toughness of through-the-thickness reinforced graphite/epoxy", *Proceedings of the 27th Structures, Structural Dynamics and Materials Conference*, 1020. https://doi.org/10.2514/6.19861020

Dransfield, K., Baillie, C. and Mai, Y.-W. (1993), "On stitching as a method for improving the delamination resistance of CFRPs", Minerals, Metals and Materials Society, Warrendale, PA, USA.

Dransfield, K., Baillie, C. and Mai, Y.-W. (1995), "Improving the delamination resistance of CFRP by stitching—a review", *Compos. Sci. Technol.*, **50**, 305-317. https://doi.org/10.1016/0266-3538(94)90019-1

Dransfield, K.A., Jain, L.K. and Mai, Y.-W. (1998), "On the effects of stitching in CFRPs—I. Mode I delamination toughness", *Compos. Sci. Technol.*, **58**, 815-827. https://doi.org/10.1016/S0266-3538(97)00229-7

Elices, M., Guinea, G.V., Gomez, J. and Planas, J. (2002), "The cohesive zone model: advantages, limitations and challenges", *Eng. Fract. Mech.*, **69**, 137-163. https://doi.org/10.1016/S0013-7944(01)00083-2

Eyvazian, A., Musharavati, F., Talebizadehsardari, P. and Sebaey, T.A. (2020), "Free vibration of FGG PLRC spherical shell on two parameter elastic foundation", *Steel Compos. Struct.*, *Int. J.*, **36**(6), 711-727. https://doi.org/10.12989/scs.2020.36.6.711

Ghaznavi, V. and Shariyat, M. (2017), "Non-linear layerwise dynamic response analysis of sandwich plates with soft auxetic cores and embedded SMA wires experiencing cyclic loadings", *Compos. Struct.*, **171**, 185-197. https://doi.org/10.1016/j.compstruct.2017.03.012

Geubelle, P.H. and Baylor, J.S. (2017), "Impact-induced delamination of composites: a 2D simulation", *Compos. Part B Eng.*, **29**, 589-602. https://doi.org/10.1016/S1359-8368(98)00013-4

Hu, F.Z., Soutis, C. and Edge, E.C. (1997), "Interlaminar stresses in composite laminates with a circular hole", *Compos. Struct.*, **37**, 223-232. https://doi.org/10.1016/S0263-8223(97)80014-1

Huebner, K.H., Dewhirst, D.L., Smith, D.E. and Byrom, T.G. (2001), *The Finite Element Method for Engineers*, John Wiley & Sons.

Ibrahim, H.H., Tawfik, M. and Negm, H.M. (2011), "Thermal buckling and nonlinear flutter behavior of shape memory alloy hybrid composite plates", *J. Vib. Control*, **17**, 321-333. https://doi.org/10.1177/1077546309353368

Jain, L.K. and Mai, Y.-W. (1994), "Analysis of stitched laminated ENF specimens for interlaminar mode II fracture toughness", *Int. J. Fract.*, **68**, 219-244. https://doi.org/10.1007/BF00013069

Jain, L.K. and Mai, Y.-W. (1995), "Determination of mode II delamination toughness of stitched laminated composites", *Compos. Sci. Technol*, **55**, 241-253. https://doi.org/10.1016/0266-3538(95)00089-5

Jankowski, J. (2008), "Dynamic response of thin-walled composite beam-columns with closed and open crosssections", *Mech. Mech. Eng.*, **12**(3), 255-265.

Khorasani, M., Eyvazian, A., Karbon, M., Tounsi, A., Lampani, L. and Sebaey, T.A. (2020), "Magnetoelectro-elastic vibration analysis of modified couple stress-based three-layered micro rectangular plates exposed to multi-physical fields considering the flexoelectricity effects", *Smart Struct. Syst.*, *Int. J.*, **26**(3), 331-343. https://doi.org/10.12989/sss.2020.26.3.331

Koning, C. and Taub, J. (1934), Impact buckling of thin bars in the elastic range hinged at both ends.

Kowal-Michalska, K. (2010), "About some important parameters in dynamic buckling analysis of plated structures subjected to pulse loading", *Mech. Eng.*, **14**, 269-279.

Kubiak, T. (2013), *Static and dynamic buckling of thin-walled plate structures*, Springer, pp. 3905-3919.

Kumar, P. and Srinivasa, C.V. (2020), "On buckling and free vibration studies of Sandwich plates and cylindrical shells: a review", *J. Thermoplast. Compos. Mater.*, **33**(5), 673-724. https://doi.org/10.1177/0892705718809810

Lau, K.T., Ling, H.Y. and Zhou, L.M. (2004), "Low velocity impact on shape memory alloy stitched composite plates", *Smart Mater. Struct.*, **13**(2), 364-370. https://doi.org/10.1088/0964-1726/13/2/015

Lee, I., Roh, J.-H. and Oh, I.-K. (2003), "Aero thermoelastic phenomena of aerospace and composite structures", *J. Therm. Stress.*, **26**, 525-546. https://doi.org/10.1080/713855957

Leissa, A.W. (1987), "A review of laminated composite plate

buckling", *Appl. Mech. Rev.*, **40**(5), 575-591. https://doi.org/10.1115/1.3149534

Li, Z. (2005), "Computational analyses and simulations of fluid-structure interactions applied to stented abdominal aortic aneurysms", North Carolina State University.

Mahieddinet, A., Ouali, M. and Mazouz, A. (2015), "Modeling and simulation of partially delaminated composite beams", *Steel Compos. Struct., Int. J.*, **18**(5), 1119-1127. https://doi.org/10.12989/scs.2015.18.5.1119

Manfredi, E., Cohades, A., Richard, I. and Michaud, V. (2014), "Assessment of solvent capsule based healing for woven E-glass fibre-reinforced polymers", *Smart Mater. Struct.*, **24**(1), 015019. https://doi.org/10.1088/0964-1726/24/1/015019

Marshall, I.H. (1987), "Membrane stress distributions in post-buckled composite plates with circular holes", *Compos. Struct.*, **4**, 557.

Massabo, R. and Cox, B.N. (1999), "Concepts for bridged mode II delamination cracks", *J. Mech. Phys. Solids.*, **47**, 1265-1300. https://doi.org/10.1016/S0022-5096(98)00107-0

Mouritz, A.P. (1995), "The flexural strength of stitched GRP laminates following underwater explosion shock loading", *Proceedings of the 10th International Conference on Composite Materials. V. Structures*, pp. 695-701.

Mouritz, A.P., Leong, K.H. and Herszberg, I. (1997), "A review of the effect of stitching on the in-plane mechanical properties of fibre-reinforced polymer composites", *Compos. Part A Appl. Sci. Manuf.*, **28**, 979-991. https://doi.org/10.1016/S1359-835X(97)00057-2

Nemeth, M.P., Stein, M. and Johnson, E.R. (1986), "An Approximate Buckling Analysis for Rectangular Orthotropic Plates with Centrally Located Cutouts", Tech. rep.

Nishimura, A. and Aotani, H. (1986), "New fabric structures for composites", *Compos. Recent Adv. Japan United States*, 29-36.

Palmer, R.J., Dow, M.B. and Smith, D.L. (1991), "Development of stitching reinforcement for transport wing panels".

Petry, D. and Fahlbusch, G. (2000), "Dynamic buckling of thin isotropic plates subjected to in-plane impact", *Thin-Wall. Struct.*, **38**, 267-283. https://doi.org/10.1016/S0263-8231(00)00037-9

Phoenix, S.L., Yavuz, A.K., Papoulia, K.D. and Hui, C.Y. (2006), "Buckling analysis of delaminated and stitched composite plate system under hygro thermal pressure", *J. Eng. Mater. Technol.*, **128**(1), 117-122. https://doi.org/10.1115/1.2128428

Qian, H., Li, H.N., Song, G., Chen, H., Ren, W.J. and Zhang, S. (1994), "Seismic vibration control of civil structures using shape memory alloys: a review", *Earth and Space 2010: Engineering, Science, Construction, and Operations in Challenging Environments*, PP. 3377-3395. https://doi.org/10.1061/41096(366)322

Reissner, E. (1944), "On the theory of bending of elastic plates", *J. Math. Phys.*, **23**, 184-191.

Riccio, A., Linde, P., Raimondo, A., Buompane, A. and Sellitto, A. (2017), "On the use of selective stitching in stiffened composite panels to prevent skinstringer debonding", *Compos. B. Eng.*, **124**, 64-75. https://doi.org/10.1016/j.compositesb.2017.05.052

Rogers, C.A., Liang, C. and Jia, J. (1991), "Structural modification of simply-supported laminated plates using embedded shape memory alloy fibers", *Comput. Struct.*, **38**(5-6), 569-580. https://doi.org/10.1016/00457949(91)90008- A

Saboori, B., Torabi, A.R., Berto, F. and Razavi, S.M.J (2018), "Averaged strain energy density to assess mixed mode I/III fracture of U-notched GPPS samples", *Struct. Eng. Mech., Int. J.*, **65**(6), 699-706. https://doi.org/10.12989/sem.2018.65.6.699

Sahmani, A. and Fattahi, A.M. (2018), "Small scale effects on buckling and postbuckling behaviors of axially loaded FGM nanoshells based on nonlocal strain gradient elasticity theory.", *Appl. Math. Mech.*, **39**, 561580. https://doi.org/10.1007/s10483-018-2321-8

Sankar, B.V. and Sharma, S. (1995), "Effects of stitching on fracture toughness of uniweave textile graphite/epoxy laminates", *NASA CONFERENCE PUBLICATION*, 481.

Shariyat, M., Moradi, M. and Samaee, S. (2014), "Enhanced model for nonlinear dynamic analysis of rectangular composite plates with embedded SMA wires, considering the instantaneous local phase changes", *J. Compos. Struct.*, **109**, 106-118. https://doi.org/10.1016/j.compstruct.2013.10.032

Sekiguchi, Y., Katano, M. and Sato, C. (2017), "Experimental study of the mode I adhesive fracture energy in DCB specimens bonded with a polyurethane adhesive", *J. Adhes.*, **93**, 235-255. https://doi.org/10.1080/00218464.2015.1070101

Soltanieh, G., Kabir, M.Z. and Shariyat, M. (2017), "Snap instability of shallow laminated cylindrical shells reinforced with functionally graded shape memory alloy wires", *Compos. Struct.*, **180**, 581-595. https://doi.org/10.1016/j.compstruct.2017.08.027

Soltanieh, G., Kabir, M.Z. and Shariyat, M. (2018), "A robust algorithm for behavior and effectiveness investigations of super-elastic SMA wires embedded in composite plates under impulse loading", *Compos. Struct.*, **179**, 355-367. https://doi.org/10.1016/j.compstruct.2017.07.065

Soltanieh, G., Kabir, M.Z. and Shariyat, M. (2019), "Improvement of the dynamic instability of shallow hybrid composite cylindrical shells under impulse loads using shape memory alloy wires", *Compos. B. Eng.*, **167**, 167-179. https://doi.org/10.1016/j.compositesb.2018.12.040

Talebizadehsardari, P., Eyvazian, A., Azandariani, M.G., Tran, T.N., Rajak, D.K. and Mahani, R.B. (2020), "Buckling analysis of smart beams based on higher order shear deformation theory and numerical method", *Steel Compos. Struct., Int. J.*, **35**(5), 635-640. https://doi.org/10.12989/scs.2020.35.5.635

Tawfik, M., Ro, J.-J. and Mei, C. (2002), "Thermal post-buckling and aeroelastic behaviour of shape memory alloy reinforced plates", *Smart Mater. Struct.*, **11**, 297. https://doi.org/10.1088/0964-1726/11/2/313

Torabi, A.R., Saboori, B. and Kmajoo, M.R. (2020), "Out-of-plane ductile failure of notch: Evaluation of Equivalent Material Concept", *Struct. Eng. Mech., Int. J.*, **75**(5), 559-569. https://doi.org/10.12989/sem.2020.75.5.559

Turvey, G.J. and Sadeghipour, K. (1987), "Compression Buckling of Anisotropic Fiber-reinforced Flat Rectangular Plates with Central Circular Cut-outs", *Proceedings of the Sixth International Conference on Composite Materials combined with the Second European Conference on Composite Materials* (*ICCM & ECCM*), 5-47.

Wang, J., Moumni, W., Zhang, W. and Zaki, W. (2017), "A thermomechanically coupled finite deformation constitutive model for shape memory alloys based on Hencky strain", *Int. J. Eng. Sci.*, **117**, 51-77. https://doi.org/10.1016/j.ijengsci.2017.05.003

Xu, X., Ma, Y., Lim, C.W. and Chu, H. (1987), "Dynamic buckling of cylindrical shells subject to an axial impact in a symplectic system", *Int. J. Solids Struct.*, **43**, 3905-3919. https://doi.org/10.1016/j.ijsolstr.2005.03.005

Yasui, Y. and Tsukamura, K. (1987), "Buckling strength of rectangular FRP plate with a hole(In the case of CFRP and GFRP cross-ply laminated plates)", *Japan Soc. Mater. Sci. J.*, **37**, 1050-1056.

Ye, L. (1988), "Role of matrix resin in delamination onset and growth in composite laminates", *Compos. Sci. Technol.*, **33**(4), 257-277. https://doi.org/10.1016/0266-3538(88)90043-7

Zare, R., Najaafi, N., Habibi, M., Ebrahimi, F. and Safarpour, H. (2020), "Influence of imperfection on the smart control frequency characteristics of a cylindrical sensor-actuator GPLRC cylindrical shell using a proportional-derivative smart

controller", *Smart Struct. Syst., Int. J.*, **26**(4), 469-480. https://doi.org/10.12989/sss.2020.26.4.469

Zhang, J., Yam, M.C., Soltanieh, G. and Feng, R. (2021), "Collapse resistance of steel frames in two-side column-removal scenario: Analytical method and design approach", *Struct. Eng. Mech., Int. J.*, **78**(4), 485-496. https://doi.org/10.12989/sem.2021.78.4.485

Zhao, W. (2011), "Mode I Delamination fracture characterization of polymeric composites under elevated temperature", Syracuse University, NY, USA.

Zhong, Z.W., Chen, R.R., Mei, C. and Pates, C.S. (1994), "Buckling and postbuckling of shape memory alloy fiber-reinforced composite plates", *ASME-PUBLICATIONS-PVP*, **293**, 115.

FC